May, 10@Qingdao_axion

Emerging axion detection in magnetoelectric materials

孙斯纯 （Sichun Sun）

北京理工大学/Beijing Institute of Technology

Based on:1911.04511, 2003.10527, 2206.13543, 2305.00877, 2309.15069 , 2309.08407 , 2405.00490, 2406.13480

With Yu Gao(IHEP), Fei Gao (BIT), Jungsong Cang(IHEP), Junxi Duan(BIT), Chang-Yin Ji(BIT), Yugui Yao(BIT), Yiming Liu(BIT), Chu-Tian Gao(BIT), Jinneng Luo(BIT), Mingqiu Li (GUCAS &BIT), Yun-Long Zhang(NAOC), Qi-Shu Yan(GUCAS), Zhijie Zhao (GUCAS &DESY), Graham White (Southampton).

INFN Istituto Nazionale di Fisica Nucleare

SAPIENZA UNIVERSITÀ DI ROMA

北京理工大学 BEIJING INSTITUTE OF TECHNOLOGY 1940

Outline

- Blackholes and axions.
- Detecting Axion by Measuring Magnetization
- Detecting Axion by Magnetoelectric Coupling

- Materials and Methods

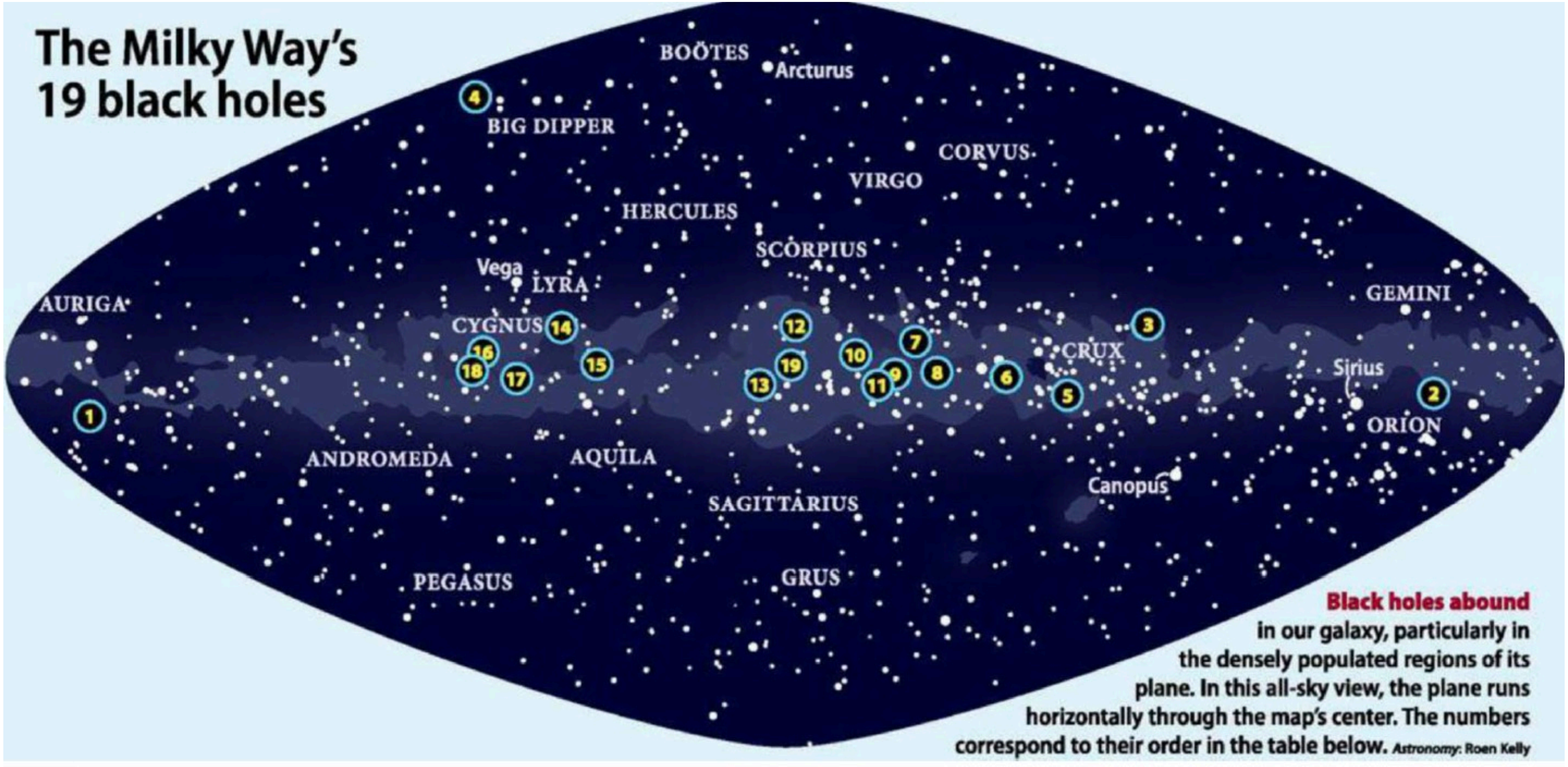

Black holes abound in our galaxy, particularly in the densely populated regions of its plane. In this all-sky view, the plane runs horizontally through the map's center. The numbers correspond to their order in the table below. *Astronomy*: Roen Kelly

Axion: scientific importance

- One very interesting dark matter candidate!
- Solving strong CP problem (Fundamental symmetry)
- **One important particle in many beyond the Standard Model extension**

$$\mathcal{L}_a = \frac{a}{f_a}\frac{g_3^2}{16\pi^2} Tr[G^{\mu}\ \widetilde{G}_{\mu}\ ]$$

- Large parameter space, tens of orders of magnitude:

$m_a \sim 10^{-5}$ eV, $f_a \sim 10^{13}$ GeV

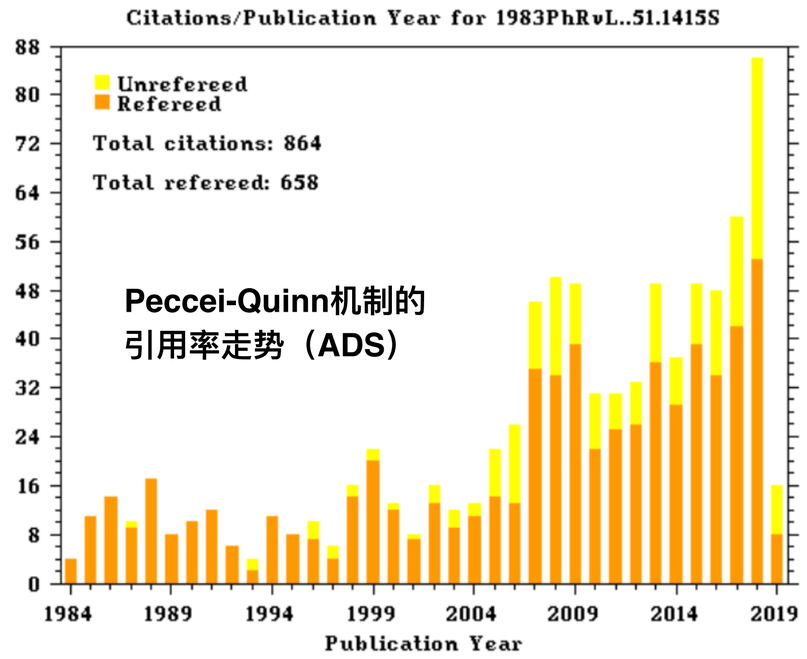

Citations on the axion paper

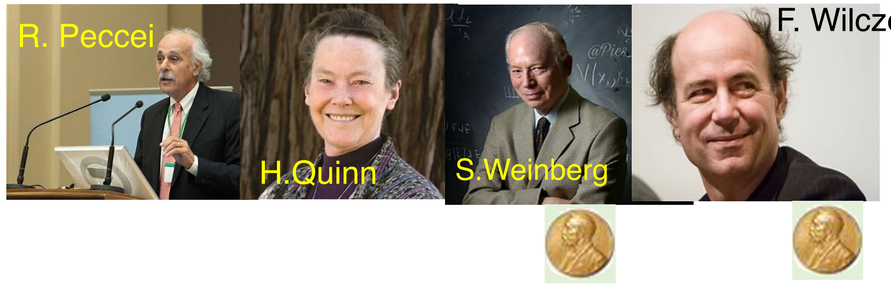

- Various detections with interdisciplinary fields and modern technology
- In condensed matter systems, axions appear as quasi-particles in certain materials,

Two different assumtions:
Axions are either coupled to photons or electrons in the materials:

$$\mathcal{L}_a = \frac{1}{2}(\partial_\mu a)(\partial^\mu a) - \frac{1}{2}m_a^2 a^2,$$

$$\mathcal{L}_{a\gamma\gamma} = -\frac{\theta_{a\gamma\gamma}}{4}F_{\mu\nu}\tilde{F}^{\mu\nu} = \theta_{a\gamma\gamma}\mathbf{E}\cdot\mathbf{B},$$

$$\rho_{\mathrm{DM}} = \frac{1}{2}m_a^2|a_0|^2,$$

$$\theta_{a\gamma\gamma} \equiv a g_{a\gamma\gamma},$$

$$\chi\theta_{ae} \equiv g_{ae}\frac{a_0 m_a \hbar}{m_e^2 c^2 g_s \alpha_E e^2}\sqrt{\frac{\varepsilon_0}{\mu_0}} \sim 7.7\times 10^{-11} g_{ae},$$

$$\delta E_{ae}^{\mathrm{tot}} \approx L_{\mathrm{domain}}^3 \chi\theta_{ae}\sqrt{\frac{\mu_0}{\varepsilon_0}}\mathbf{P}\cdot\mathbf{M},$$

According to the Ginzburg-Landau theory

$$\mathcal{F}[\mathbf{M},\mathbf{P}] = \mu_0\mathcal{F}_M[\mathbf{M}] + \frac{1}{\varepsilon_0}\mathcal{F}_P[\mathbf{P}] - \sqrt{\frac{\mu_0}{\varepsilon_0}}(\alpha_{ij}M^iP^j + \chi\theta\mathbf{P}\cdot\mathbf{M}),$$

$$\mathcal{F}_M[\mathbf{M}] = \alpha_M|\partial_t\mathbf{M}|^2 - \beta_M|\nabla\cdot\mathbf{M}|^2 - \gamma_M(T-T_{C_M})|\mathbf{M}|^2 - \lambda_M|\mathbf{M}|^4 + \ldots,$$

$$\mathcal{F}_P[\mathbf{P}] = \alpha_P|\partial_t\mathbf{P}|^2 - \beta_P|\nabla\cdot\mathbf{P}|^2 - \gamma_P(T-T_{C_P})|\mathbf{P}|^2 - \lambda_P|\mathbf{P}|^4 + \ldots,$$

$$\alpha_M\ddot{M} + \gamma_M(T-T_{C_M})M + 2\lambda_M M^3 + \frac{c}{2}(\alpha+\chi\theta)P = 0,$$

$$\alpha_P\ddot{P} + \gamma_P(T-T_{C_P})P + 2\lambda_P P^3 + \frac{1}{2c}(\alpha+\chi\theta)M = 0.$$

$$\left|\frac{\delta M}{\theta_0}\right| = \frac{\chi\sqrt{4c^2P_0^2\alpha_P^2\eta_P^2\omega_a^2 + [M_0\alpha + 2cP_0(\alpha_P\omega_a^2 - m_P^2)]^2}}{\sqrt{16\omega_a^2[\alpha_M\alpha_P\omega_a^2(\eta_M+\eta_P) - \alpha_P\eta_P m_M^2 - \alpha_M\eta_M m_P^2]^2 + [\alpha^2 + 4\alpha_M\alpha_P\eta_M\eta_P\omega_a^2 - 4(\alpha_M\omega_a^2 - m_M^2)(\alpha_P\omega_a^2 - m_P^2)]^2}}.$$

$$m_M^2 \equiv \gamma_M(T-T_{C_M}) + 6\lambda_M M_0^2,$$

where ω_M is the magnetic (magnon) frequency with definition:

$$\omega_M^2 \equiv \frac{1}{\alpha_M}[m_M^2 - \frac{\alpha^2}{4m_P^2}].$$

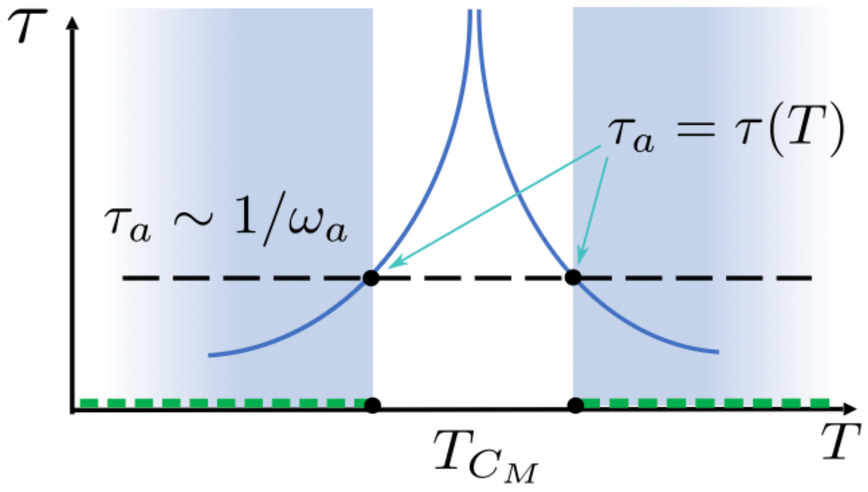

FIG. 2. Sketch of critical slowing down for the magnetization dynamics time scale τ (blue curve). The horizontal dashed line indicates the steady axion dynamics time scale τ_a. Temperature tuning can be used to match the magnetic time scale with the axion time scale. The adiabatic regime away from the critical point, where axion dynamics is slow compared to magnetization time scale $\tau < \tau_a$, is shown with a green dashed lines on the temperature axis.

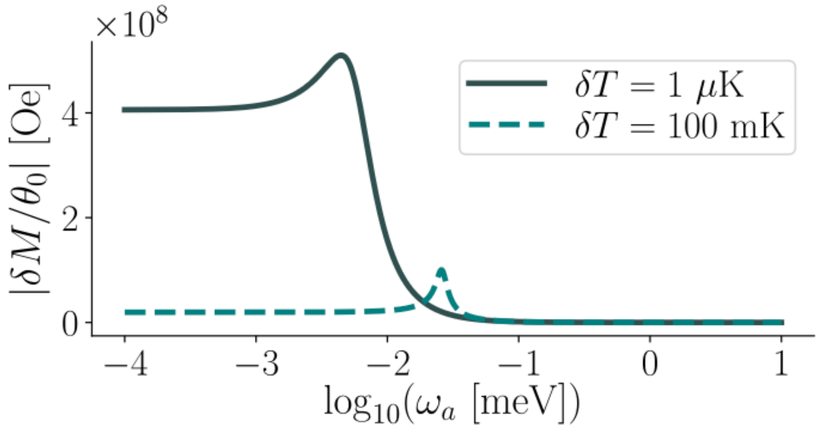

FIG. 3. The magnetic linear response for axions coupling to ferroic orders, for two values of $\delta T = T_{C_M} - T$. Dynamical frequency response from Eq. (10) assuming that $\alpha_M^{-1} = (1\,\text{meV})^2$ and $\eta_M = 5\,\mu\text{eV}$. Here we used the parameters $\chi = 1$, $m_P = 4.5 \times 10^{-2}$, $\alpha_0 = 10^{-3}$, $b = 0.4$, $\gamma_M = 10^{-5}\,\text{K}^{-1}$, $\lambda_M = 9.25\,\text{kOe}^{-2}$, $P_0 = 0.7\,\mu\text{C/cm}^2$, and $T_{C_M} = 160\,\text{K}$, as roughly motivated by the compound h-LSFO, see the main text and Sec. IV.

Detecting Axion by Magnetoelectric Coupling

- reflection high-energy electron diffraction (RHEED)
- Measuring the axion number directly:

$$\theta_{tot} = \theta_0 + \theta.$$

$$\alpha_{ij} = \frac{\partial P}{\partial H}|_{\mathbf{E}=0}. \qquad \theta = \frac{4\pi^2\hbar c\alpha_{ij}}{e^2}.$$

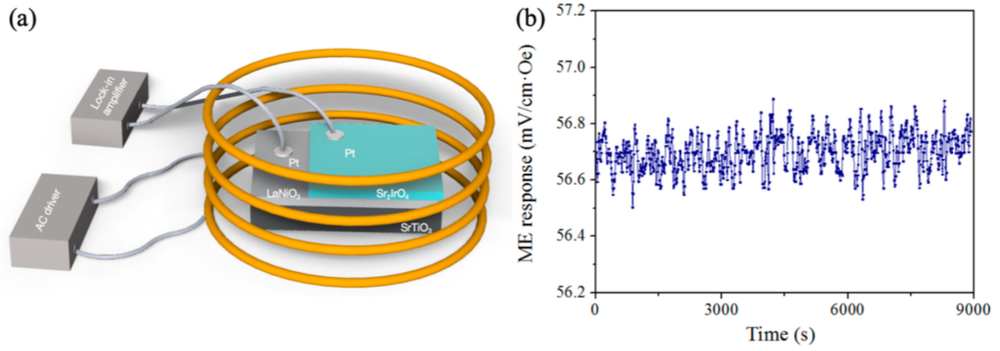

Figure 3: (a) Schematic of the magnetoelectric coupling measurement system. An alternating current is applied to generate an alternating magnetic field, and a lock-in amplifier detects the alternating electrical signal induced in the sample.(b) Time-dependent magnetoelectric response curve at 20 K.

Sr_2IrO_4 is an iridate material characterized by strong spin-orbit coupling,

Future projection:

With the limits:

$$\mathrm{SNR} \sim \frac{V}{\gamma T} \frac{|P_0|^2}{\Delta\omega_a \alpha_M} (\chi\theta)^2 \sqrt{\frac{\Delta\omega_a}{\Delta\omega_{\mathrm{meas}}}}$$

Several scales:

$$\mathrm{SNR} \propto \left(\frac{t_{\mathrm{meas}}}{t_{\mathrm{coh}}}\right)^{1/2} . \quad t_{\mathrm{coh}} \sim 10^6 \cdot \left(\frac{2\pi}{\omega_a}\right)$$

There are three relevant bandwidths in the problem:

- $\gamma \sim 10^{-6}$eV the width of the magnetic resonance: our numerical estimate here are based on inelastic neutron scattering measurements[2]
- $\Delta\omega_a \sim \frac{1}{2}\omega_a v_a^2 \sim 10^{-12}$eV the width of the axion signal, expected to be determined by Doppler broadening of the Galactic axion background
- $\Delta\omega_{\mathrm{meas}} \sim t_{\mathrm{meas}}^{-1} \sim 10^{-18}$eV the measurement bandwidth, which is determined by the measurement time t_{meas}: this estimate assumes $t_{\mathrm{meas}} \sim$ 1hr.

We therefore see that $\gamma \gg \Delta\omega_a \gg \Delta\omega_{\mathrm{meas}}$. In this regime the signal-to-noise ratio is[3,4]

$$\frac{S}{N} = \frac{S_\theta(\omega_a)}{S_\xi(\omega_a)} \sqrt{\frac{\Delta\omega_a}{\Delta\omega_{\mathrm{meas}}}} \qquad (4)$$

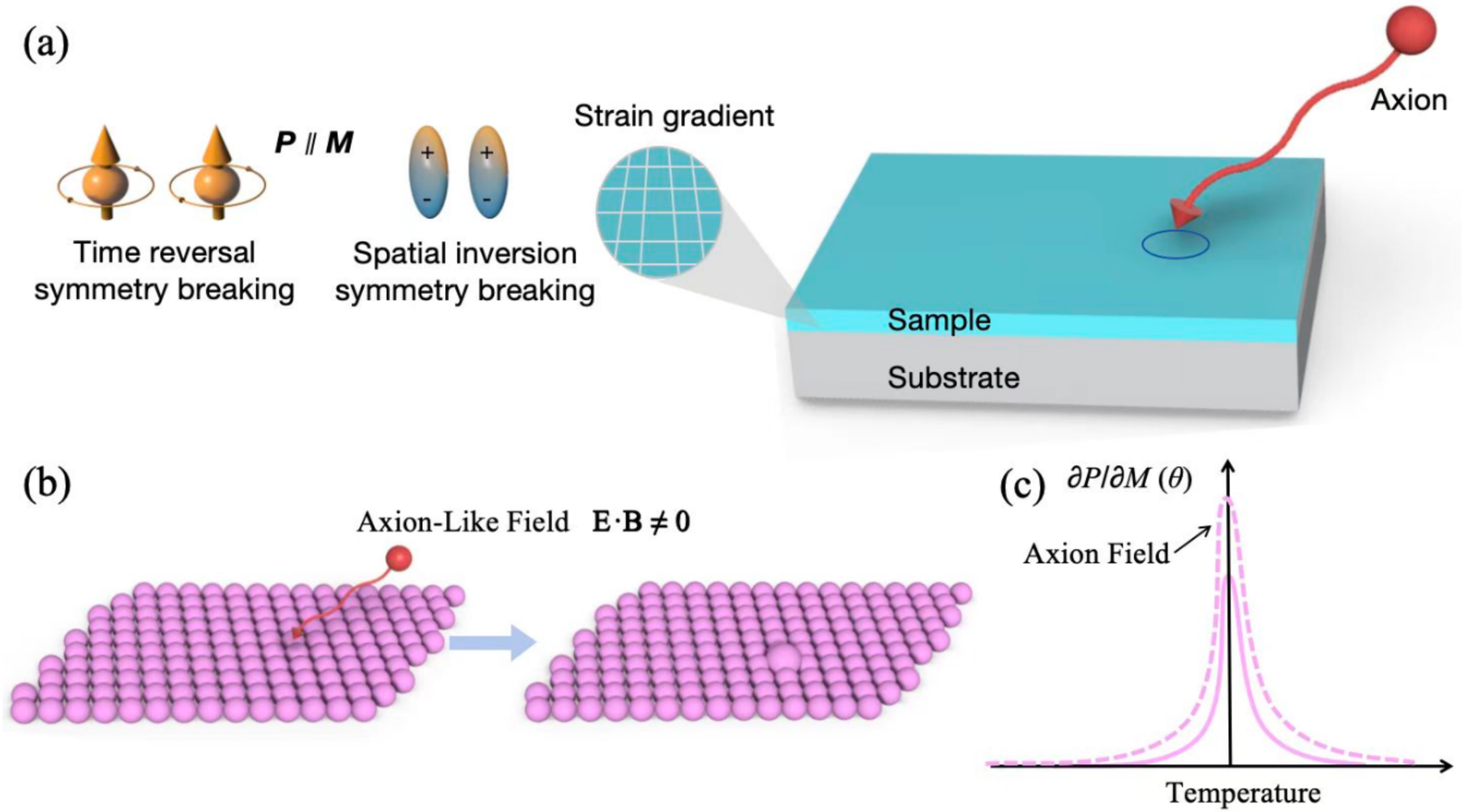

Figure 1: (a) The magnetoelectric material exhibits parallel polarization (P) and magnetization (M), corresponding to the breaking of spatial inversion symmetry and time-reversal symmetry. (b) Enlarged view within the circle of (a), where the external axion field effectively couples with the internal axion-like field in the material. (c) The magnetoelectric coupling effect is significantly enhanced after applying the external axion field.

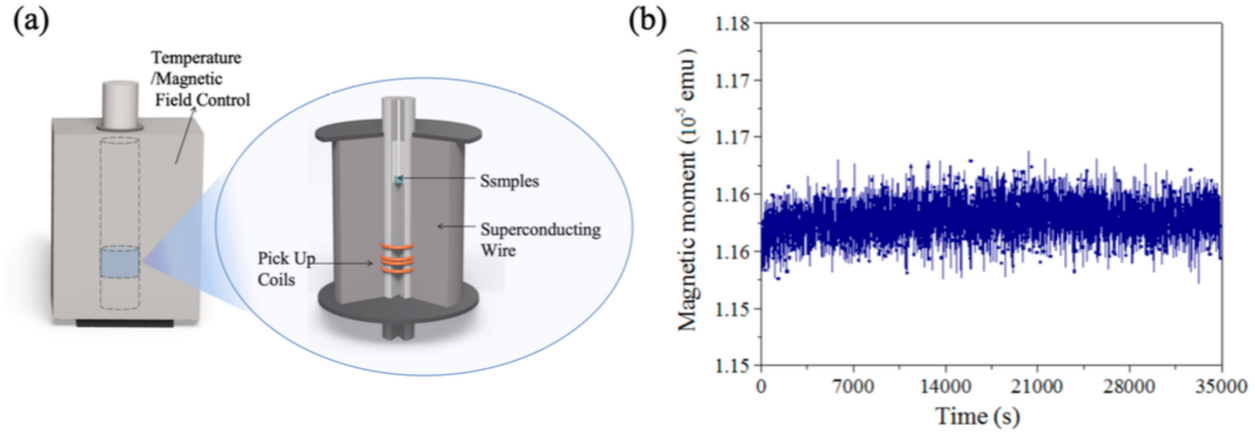

Figure 2: (a) Schematic of the SQUID measurement system, when the sample moves in the center, the magnetic flux through the coil changes, inducing an electromotive force, which in turn allows the determination of the sample's magnetic moment. (b) Time-dependent magnetization curve at 20 K.

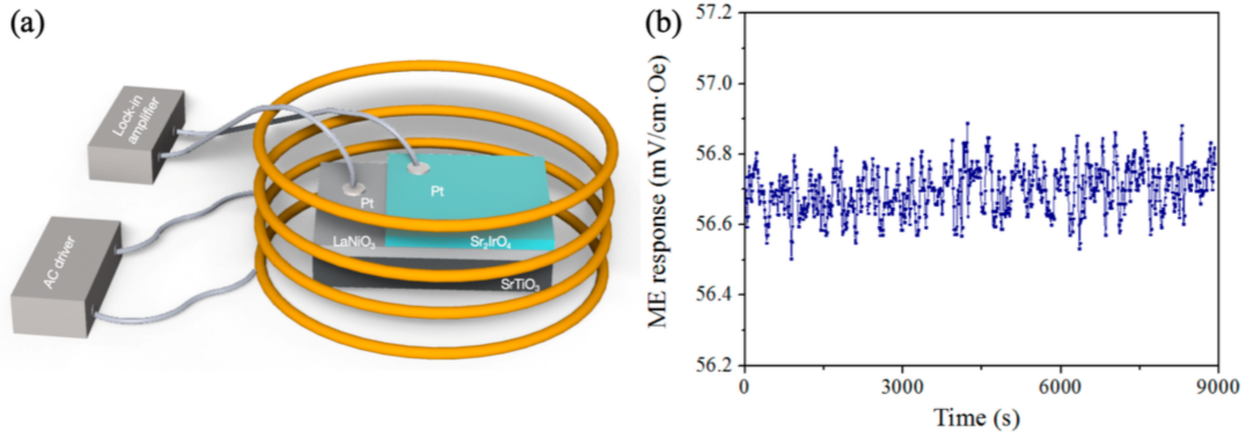

Figure 3: (a) Schematic of the magnetoelectric coupling measurement system. An alternating current is applied to generate an alternating magnetic field, and a lock-in amplifier detects the alternating electrical signal induced in the sample.(b) Time-dependent magnetoelectric response curve at 20 K.

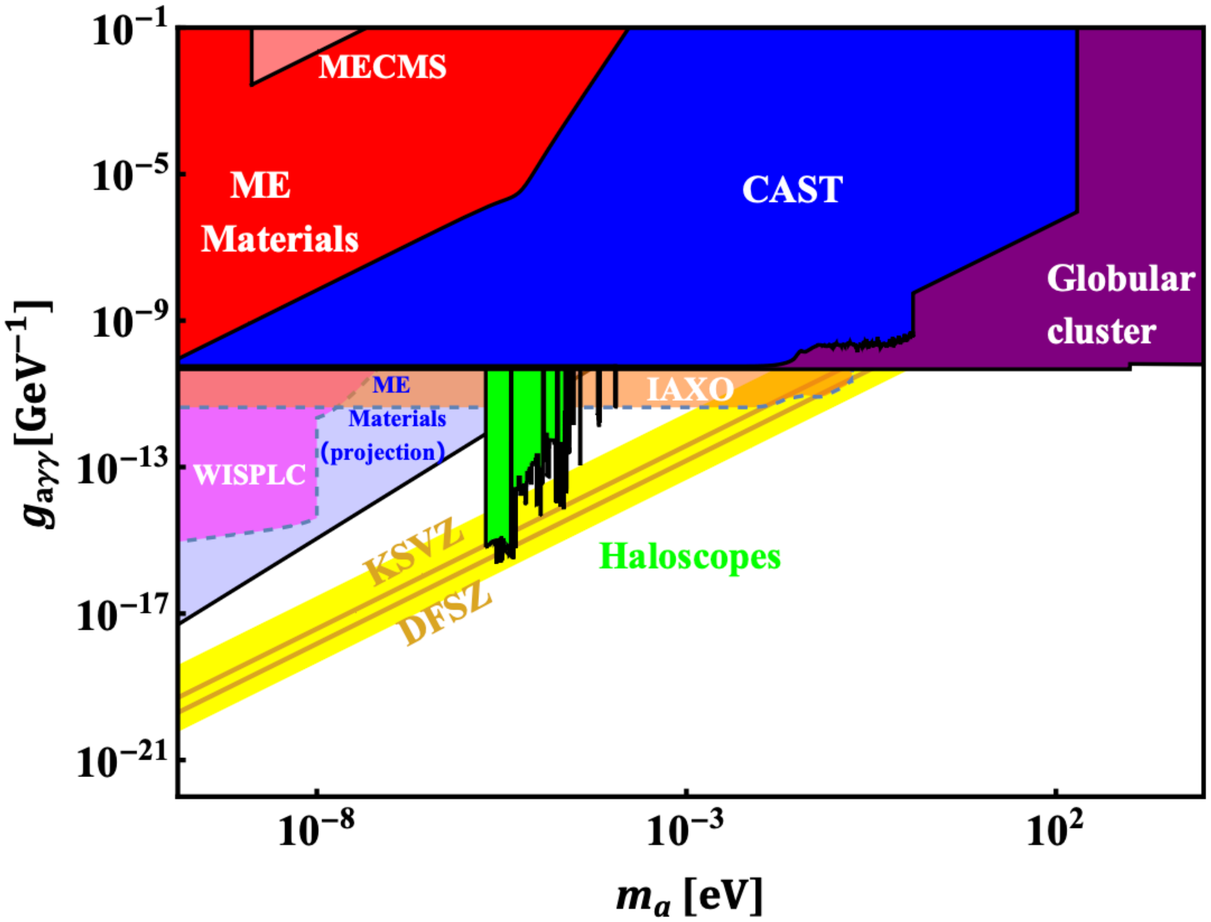

Figure 4: Constraints on the coupling factor $g_{a\gamma\gamma}$. The red and pink exclusion is obtained by our experiments, where we use an external magnetic field around 1000 Oe. The size of the test sample is 300 nm $\times$ 2.5 mm $\times$ 2.5 mm. The SQUID measurement system obtains the red exclusion, and the magnetoelectric coupling measurement system (MECMS) obtains the pink exclusion. For the red exclusion, the integration time of M is 10 seconds, while for the pink exclusion, the integration time of θ is 1 second. The projection of Magnetoelectric Materials is made assuming SNR=3. The size of the magnetoelectric material sample for the projection is $0.1 \times 0.1 \times 0.01$ m^3. The integration time of the projection is one year. We consider the 95% C.L. exclusion limit. The bound of the Globular cluster comes from Reference [60]. The bound of CAST comes from Reference [61]. The projection of WISPLC comes from Reference [62]. The projection of IAXO comes from Reference [63]. The yellow lines represent KimShifman-Vainshtein-Zakharov (KSVZ) and Dine-FischlerSrednicki-Zhitnitsky (DFSZ) axion models, and the yellow region represents the hadronic band. The trend showing improved sensitivity to $g_{a\gamma}$ at lower ALP masses (frequencies) is due to the narrowing linewidth of the ALP signal [15].

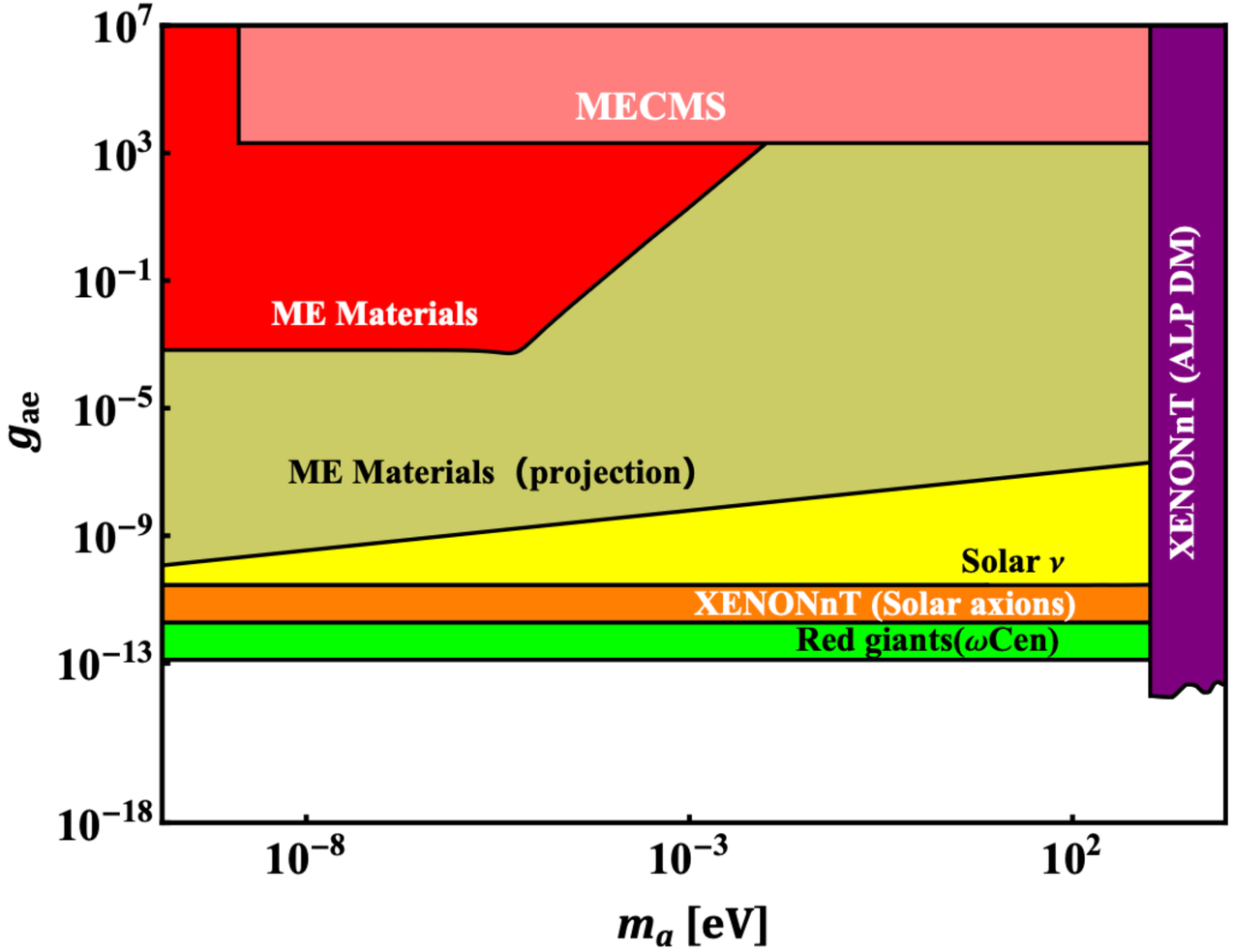

Figure 5: Constraints on the coupling factor g_{ae}. The red and pink exclusion is obtained by our experiments, where we use an external magnetic field around 1000 Oe. The SQUID measurement system obtains the red exclusion, and the magnetoelectric coupling measurement system (MECMS) obtains the pink exclusion. The size of the test sample is 300 nm $\times$ 2.5 mm $\times$ 2.5 mm. For the red exclusion, the integration time of M is 10 seconds, while for the pink exclusion, the integration time of θ is 1 second. The projection of Magnetoelectric Materials is made assuming SNR=3. The size of the magnetoelectric material sample for the projection is $0.1 \times 0.1 \times 0.01$ m^3. The integration time of the projection is one year. We consider the 95% C.L. exclusion limit. The bounds of XENONnT (Solar axions) and XENONnT (ALP DM) come from Reference [58]. The Red giant branch bound is taken from Reference [59]. The constraint of Solar neutrinos comes from Reference [14].

- Thanks.